One- and Two-Electron Oxidative Pathways Leading to Cyclopropane-Containing Oxidized Porphyrinogens and C−C-Coupled Porphyrinogens from Alkali Cation− and Transition Metal−*meso*-Octaethylporphyrinogen Complexes

Raffaella Crescenzi,[†] Euro Solari,[†] Carlo Floriani,*[,†] Angiola Chiesi-Villa,[‡] and Corrado Rizzoli[‡]

Contribution from the Institut de Chimie Minérale et Analytique, BCH, Université de Lausanne, CH-1015 Lausanne, Switzerland, and Dipartimento di Chimica, Università di Parma, I-43100 Parma, Italy

Received June 22, 1998

Abstract: This report deals with the different transition metal- and alkali cation-assisted oxidation pathways of the *meso*-octaethylporphyrinogen tetraanion $[Et_8N_4]^{4-}$. The two-electron oxidation of $[Et_8N_4Mn\{Na(thf)_2\}_2]$, **4**, with Cp_2FeBPh_4 led to the corresponding monocyclopropane derivative $[Et_8N_4(\Delta)Mn]$, **6**, [$\Delta \equiv$ cyclopropane], while the one-electron oxidation with $CuCl_2$ or O_2 led to the Mn(III)−porphyrinogen $[Et_8N_4Mn][Li(thf)_4]$, **5**, which can be further oxidized by an excess of $CuCl_2$ to $[Et_8N_4(\Delta)_2Mn-Cl]^+[Cu_9Cl_{11}]_{0.5}$, **7**. The formation of **7** does not follow the expected sequence Mn(II) → Mn(III) → Mn(II)−monocyclopropane → Mn(II)−biscyclopropane−porphyrinogen. In the case of iron(II)−porphyrinogen, $[Et_8N_4Fe\{Li(thf)_2\}_2]$, **9**, the oxidation led in a preliminary stage to the iron(III) derivative $[Et_8N_4Fe][Li(thf)_4]$, **10**, then to the metalated form of the biscyclopropane−porphyrinogen $[Et_8N_4(\Delta)_2Fe-Cl]\{\mu\text{-}Cu_4Cl_5\}]$, **11**. The supposed stabilization of the biscyclopropane by the copper(I) cluster was ruled out by carrying the oxidation of $[Cy_4N_4Fe\{Li(thf)_2\}_2]$, **11**, to $[Cy_4N_4(\Delta)_2Fe-Cl][Cu_2Cl_4]$, **14**. The stepwise oxidation of $[Et_8N_4M(thf)_4]$ [M = Li, **1**; M = Na, **2**] with Cp_2FeBPh_4 led to $[Et_8N_4(\Delta)Li_2thf_2]$, **15**, $[Et_8N_4(\Delta)Li]BPh_4$, **16**, and $[Et_8N_4(\Delta)Na]BPh_4$, **17**. The reaction of **1** with **16** leading to **15** showed how the C−C moiety in cyclopropane can be engaged in an intermolecular electron transfer. The reaction of **17** with 18-crown-6 allowed the release of biscyclopropane−porphyrinogen $[Et_8N_4(\Delta_2)]$. Particularly interesting is the thermal rearrangement of **15** to **19** occurring via intra- and intermolecular electron transfers with the transposition of the C−C bond of the cyclopropane to a C−C bridge across the β position of two adjacent pyrroles. In the case of metals, such as Ni(II), which do not undergo oxidation state changes, the primary oxidation product of a metalla-*meso*-octaalkylporphyrinogen is the monocyclopropane derivative, which reacting with the starting material masks an overall one-electron oxidation. In fact, the reaction of $[Et_8N_4Ni\{Li(thf)_2\}_2]$, **20**, with 2 equiv of Cp_2FeBPh_4 led to the expected $[Et_8N_4(\Delta)Ni]$, **21**, while the reaction of **20** with 1 equiv of Cp_2FeBPh_4 led to the dimer $[(\beta-\beta)(Et_8N_4)_2Ni_2]$, **22**, which forms equally well from the reaction of **20** and **21**. Complex **22** is a quite unique metallaporphyrinogen dimer, where the two monomeric units are joined via a C−C bond in the β position of a pyrrole. Such a reaction shows that the methodology can accede to oligomeric forms of metallaporphyrinogens.

Introduction

A porphyrin skeleton forms from a six-electron oxidation of porphyrinogen, as exemplified in Chart 1, with the loss of six hydrogen atoms.[1] However, the high tendency of the *meso*-tetrahydrotetraalkylporphyrinogen to autoxidize to porphyrin prevented inspection of such a fundamental reaction and trapping of other oxidized forms of porphyrinogen which can have relevant mechanistic and synthetic properties. To this purpose, we approached the problem by studying the various aspects of the oxidation of a stable porphyrinogen, namely, the *meso*-octaalkylporphyrinogen in its tetraanionic form, when bonded to a transition metal that can assist the process.[2,3]

In the absence of any hydrogen in the *meso* positions and within the N_4 core the oxidation of the *meso*-octaalkylporphyrinogen−metal complexes led to two- and four-electron oxidation (see **B** and **C** in Chart 2) with the introduction of one, then two cyclopropane units, hereinafter abbreviated as $\Delta \equiv$ cyclo-

Chart 1

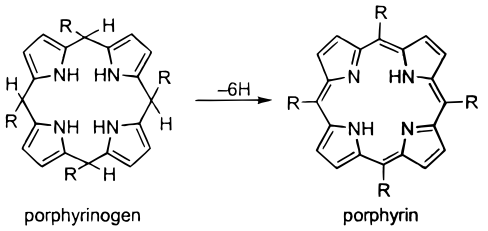

* To whom correspondence should be addressed.

[†] Université de Lausanne.

[‡] Università di Parma.

(1) (a) *The Porphyrins*; Dolphin, D., Ed.; Academic Press: New York, 1978; Vols. 1−7. (b) Smith, K. M. *Porphyrins and Metalloporphyrins*; Elsevier: Amsterdam, 1975.

(2) (a) De Angelis, S.; Solari, E.; Floriani, C.; Chiesi-Villa, A.; Rizzoli, C. *J. Am. Chem. Soc.* **1994**, *116*, 5691. (b) De Angelis, S.; Solari, E.; Floriani, C.; Chiesi-Villa, A.; Rizzoli, C. *J. Am. Chem. Soc.* **1994**, *116*, 5702. (c) Jubb, J.; Floriani, C.; Chiesi-Villa, A.; Rizzoli, C. *J. Am. Chem. Soc.* **1992**, *114*, 6571.

(3) (a) Floriani, C. *Chem. Commun.* **1996**, 1257. (b) Floriani, C. In *Transition Metals in Supramolecular Chemistry*; Fabbrizzi, L., Poggi, A., Eds.; Kluwer: Dordrecht, The Netherlands, 1994; Vol. 448, p 191.

10.1021/ja982178f CCC: $18.00
Published on Web 02/09/1999

Chart 2

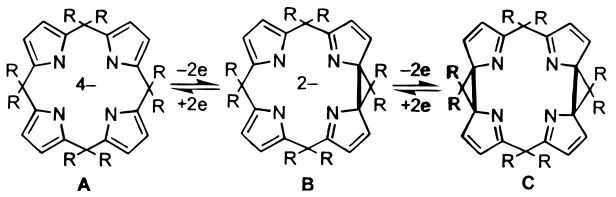

propane, within the porphyrinogen skeleton.[2,3] The monocyclopropane forms with a variety of transition metals, Ni, Cu, Co, using *p*-benzoquinone as the oxidizing agent,[2a] while the biscyclopropane form occurs only in the case of Co and Fe, when $CuCl_2$ is employed.[2b] In some cases, the use of high oxidation state metals induces the intramolecular or intermolecular formation of cyclopropane units. In the present paper we report the pathway leading to the Mn− and Fe−porphyrinogen complexes containing cyclopropane units. Cp_2FeBPh_4 enabled us to establish the oxidative pathway leading to the transition metal-free monocyclopropane, then to the biscyclopropane−porphyrinogen (**C**), which becomes available now by means of a quite convenient, large-scale, synthetic process. Another remarkable aspect covered by this paper is the intramolecular and intermolecular electron transfer occurring from the cleavage of the C−C bond of the cyclopropane functionality and formation of a C−C bond across the two β instead of α positions of two adjacent pyrroles. The electron transfer in cyclopropane-containing porphyrinogen is very often accompanied by the cleavage and formation of C−C bonds.[2,4] When such an event occurs intermolecularly, the one-electron oxidation of the porphyrinogen is achieved with the consequent oxidative coupling of two metallaporphyrinogens. This observation established the synthetic methodology for the oligomerization and polymerization of the metallaporphyrinogen moiety.

The synergetic metal-to-ligand interaction in the porphyrinogen derivative containing a cyclopropane moiety allowed a quite novel strategy for masking unusually high oxidation states for metals; thus the metal in complexes **D** can either behave as metal(II) or metal(IV)[3a] depending on the reaction pathway in which it is engaged (Chart 3). The relevance of the reversible

Chart 3

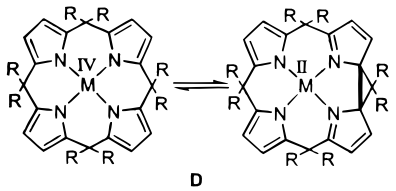

formation and cleavage of the C−C bond in porphyrinogens is not at all limited to such molecular skeletons. We should mention in this context that a few chemical systems function as "molecular batteries", storing and releasing electrons via the formation and cleavage of C−C bonds.[5]

Experimental Section

General Procedure. All reactions were carried out under an atmosphere of purified nitrogen. Solvents were dried and distilled before use by standard methods. Infrared spectra were recorded with a Perkin-Elmer FT 1600 spectrophotometer. NMR spectra were recorded on a 200-AC Bruker instrument. Magnetic susceptibility measurements were collected in the temperature range 80−300 K on a MPMS5 SQUID susceptometer (Quantum Design Inc.) operating at a magnetic field strength of 3 kOe. Corrections were applied for diamagnetism calculated from Pascal constants. The synthesis of **1**[6] and **20**[6] was carried out as reported, while a procedure modified from that reported was employed for **9**,[2b] **10**,[2b] **11**,[2b] and **12**.[7]

Synthesis of 2. Degassed naphthalene (10.36 g, 80 mmol) and then sodium (3.68 g, 160 mmol) were added to a yellow solution of $[Et_8N_4H_4]$[8] (21.64 g, 40 mmol) in THF (250 mL), resulting in a green solution, which was stirred at room temperature until the sodium had completely dissolved. THF was evaporated under reduced pressure and the resulting white solid collected with *n*-hexane (300 mL), filtered, and dried (25 g, 81%). Anal. Calcd for $C_{44}H_{64}N_4Na_4O_2$: C, 68.37; H, 8.35; N, 7.25. Found: C, 68.55; H, 8.53; N, 7.03. ^{1}H NMR (C_5D_5N, 200 MHz, 298 K, ppm): δ 6.42 (s, 8H, C_4H_2N); 3.67 (m, 8H, THF); 2.32 (m, 16H, CH_2); 1.65 (m, 8H, THF); 0.99 (m, 24H, CH_3).

Synthesis of 3. $[MnCl_2(thf)_{1.5}]$ (1.56 g, 6.7 mmol) was added to a colorless solution of **1** (5.8 g; 6.8 mmol) in benzene (250 mL), resulting in a milky suspension, which was reacted for 48 h at room temperature, then filtered to remove LiCl. The solvent was evaporated to dryness under reduced pressure and the pale pink solid collected with *n*-hexane (200 mL), filtered, and dried (4.2 g, 63%). Anal. Calcd for $C_{52}H_{80}Li_2MnN_4O_4$: C, 69.87; H, 9.19; N, 6.27. Found: C, 69.47; H, 8.88; N, 6.34. IR (Nujol, ν_{max}/cm^{-1}): 3089 (s), 1260 (s), 1047 (m), 890 (m), 830 (s), 750 (m). $\mu_{eff} = 5.91\ \mu_B$ at 293 K.

Synthesis of 4. $[MnCl_2(thf)_{1.5}]$ (2.94 g; 12.6 mmol) was added to a yellow solution of **2** (9.8 g; 12.7 mmol) in THF (250 mL), resulting in a suspension, which was stirred for 24 h at room temperature. The suspension slowly turned orange, while a thin white solid (NaCl) formed, which was removed by filtration. The solution was taken to dryness and the pink-white solid collected with *n*-hexane (150 mL), filtered, and dried (6.91 g, 67%). Anal. Calcd for $C_{52}H_{80}MnN_4Na_2O_4$: C, 67.44; H, 8.71; N, 6.05. Found: C, 67.42; H, 8.77; N, 6.26. IR (Nujol, ν_{max}/cm^{-1}): 3069 (s), 1319 (s), 1288 (w), 1233 (w), 1045 (s), 967 (m), 883 (m), 844 (m), 746 (m). $\mu_{eff} = 6.19\ \mu_B$ a 293 K.

Synthesis of 5. $[MnCl_2(thf)_{1.5}]$ (3.5 g, 15.0 mmol) was added to a solution of **1** (13.19 g, 15.5 mmol) in toluene (250 mL), resulting in a milky suspension, which was reacted for 24 h at room temperature. Then $[CuCl_2(thf)_{0.5}]$ (2.55 g, 15 mmol) was added, immediately giving a red suspension, which was stirred for 1 day. The solvent was evaporated at reduced pressure, and the red-brown solid was suspended in benzene (250 mL) and refluxed for 24 h. After the removal of salts by filtration, the red solution was taken to dryness and the resulting solid dissolved in THF (100 mL), treated with *n*-hexane (200 mL), filtered, and dried (8.41 g, 61%). Anal. Calcd for $C_{52}H_{80}LiMnN_4O_4$: C, 70.41; H, 9.09; N, 6.32. Found: C, 70.45; H, 9.15; N, 6.30. IR (Nujol, ν_{max}/cm^{-1}): 3088 (s), 1318 (m), 1246 (s), 1151 (s), 1076 (s), 1040 (s), 885 (s), 747 (s). $\mu_{eff} = 5.00\ \mu_B$ at 293 K.

Synthesis of 6. Degassed Cp_2FeBPh_4 (5.15 g, 10.0 mmol) was added to a THF (200 mL) solution of **4** (4.72 g, 5.1 mmol), cooled to −40 °C, obtaining a red solution, which was allowed to react for 24 h at room temperature. The color slowly turned purple-red. The solvent was evaporated to dryness under reduced pressure and the resulting solid extracted with Et_2O (100 mL). The product obtained after evaporation of the mother liquor was treated with pentane (50 mL), filtered, and dried (1.7 g, 56%). Anal. Calcd for $C_{44}H_{64}MnN_4O_2$: C, 71.81; H, 8.77; N, 7.61. Found: C, 71.52; H, 8.51; N, 7.59. IR (Nujol, ν_{max}/cm^{-1}): 3088 (s), 1568 (s), 1236 (s), 1105 (s), 1072 (s), 1044 (s), 1002 (s), 816 (s), 746 (s). $\mu_{eff} = 5.67\ \mu_B$ at 293 K.

Synthesis of 7. $[CuCl_2(thf)_{0.5}]$ (1.8 g, 10.6 mmol) was added to a red solution of **5** (2.2. g; 2.5 mmol) in THF (70 mL). The color faded, while an orange-yellow microcrystalline solid formed. The suspension was stirred for 24 h at room temperature, then the volume was reduced

(4) Piarulli, U.; Solari, E.; Floriani, C.; Chiesi-Villa, A.; Rizzoli, C. *J. Am. Chem. Soc.* **1996**, *118*, 3634.

(5) Gallo, E.; Solari, E.; Re, N.; Floriani, C.; Chiesi-Villa, A.; Rizzoli, C. *J. Am. Chem. Soc.* **1997**, *119*, 5144. Solari, E.; Maltese, C.; Franceschi, F.; Floriani, C.; Chiesi-Villa, A.; Rizzoli, C. *J. Chem. Soc., Dalton Trans.* **1997**, 2903. De Angelis, S.; Solari, E.; Gallo, E.; Floriani, C.; Chiesi-Villa, A.; Rizzoli, C. *Inorg. Chem.* **1996**, *35*, 5995.

(6) Jubb, J.; Jacoby, D.; Floriani, C.; Chiesi-Villa, A.; Rizzoli, C. *Inorg. Chem.* **1992**, *31*, 1306.

(7) Brown, W. H.; Hutchinson, B. J.; MacKinnon, M. H. *Can. J. Chem.* **1971**, *49*, 4017.

(8) Jacoby, D.; Floriani, C.; Chiesi-Villa, A.; Rizzoli, C. *J. Am. Chem. Soc.* **1993**, *115*, 3595, and references therein.

Scheme 1

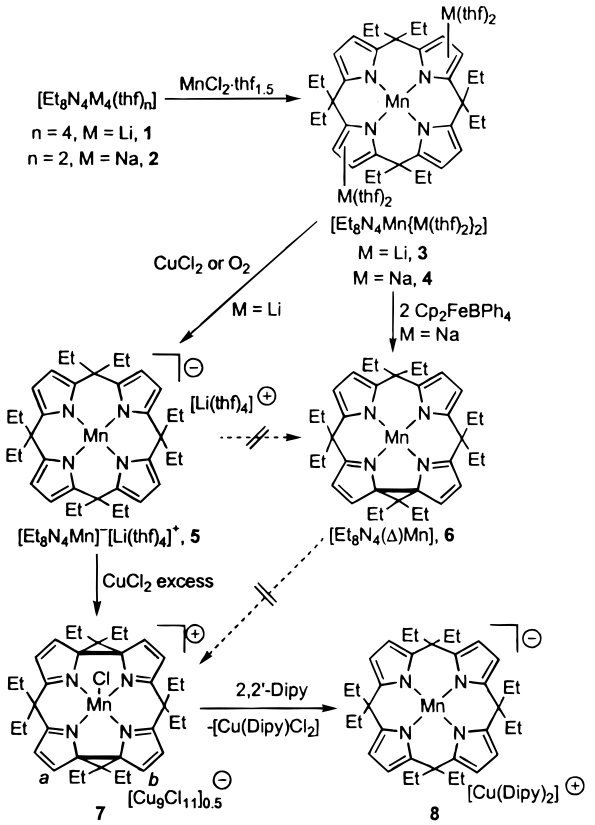

to ∼50 mL, and the resulting solid was filtered and dried (1.7 g, 61%). Anal. Calcd for $C_{72}H_{96}Cl_{13}Cu_9Mn_2N_8$: C, 39.02; H, 4.37; N, 5.06. Found: C, 39.41; H, 4.81; N, 4.45. IR (Nujol, ν_{max}/cm^{-1}): 3055 (s), 1562 (m), 1538 (m), 1046 (s), 961 (s), 814 (s). $\mu_{eff} = 5.95\ \mu_B$ at 293 K.

Synthesis of 8. A solution of 2,2′-bipyridyl (1.5 g, 10 mmol) in THF (80 mL) was reacted with **7** (0.9 g, 0.4 mmol) and the mixture stirred at room temperature for 2 h. A pale green solid formed, which was filtered off from a red solution, dried (0.70 g), and analyzed to be [($CuCl_2$)(2,2′-bipyridyl)]. Anal. Calcd for $C_{10}H_8Cl_2CuN_2$: C, 41.33; H, 2.77; N, 9.64. Found: C, 42.02; H, 2.97; N, 9.35. From the red solution, after addition of Et_2O (70 mL), a red crystalline solid precipitated (0.50 g), which was analyzed by X-ray characterization as $[Et_8N_4Mn^{III}]^-[Cu(2,2'bipy)_2]^+$. IR (Nujol ν_{max}/cm^{-1}): 3058 (m), 1595 (s), 1570 (w), 1318 (s), 1240 (s), 1151 (s), 1077 (s), 1027 (w), 972 (w), 924 (w), 882 (w), 858 (w), 807 (w), 755 (s), 734 (w), 718 (w).

Synthesis of 9. [$FeCl_2(thf)_{1.5}$] (1.29 g, 5.5 mmol) was added very slowly in a drybox to a solution of **1** (4.9 g; 5.7 mmol) in THF (250 mL), resulting in a pale yellow solution, which reacted for 5 h at room temperature. The solution was taken to dryness and the solid collected with Et_2O (250 mL) and extracted with the mother liquor. After reducing the volume of the ether, the product was filtered and dried (3.1 g, 61%). Anal. Calcd for $C_{52}H_{80}FeLi_2N_4O_4$: C, 69.79; H, 9.00; N, 6.26. Found: C, 69.51; H, 8.73; N, 5.91.

Synthesis of 10. [$FeCl_2(thf)_{1.5}$] (13.0 g, 55.4 mmol) was added to a solution of **1** (23.61 g; 27.7 mmol) in THF (500 mL), resulting in a dark red solution that reacted for 24 h at room temperature. The solution was taken to dryness and the dark red solid extracted with Et_2O (250 mL) to remove LiCl. After reducing the volume of the ether, the product was filtered and dried (23.34 g, 95%). Anal. Calcd for $C_{52}H_{80}FeLiN_4O_4$: C, 70.33; H, 9.31; N, 6.31. Found: C, 70.21; H, 9.44; N, 6.19. IR (Nujol, ν_{max}/cm^{-1}): 3088 (s), 1317 (s), 1283 (m), 1235 (s), 1150 (s), 1072 (s) 1039 (s), 883 (m), 774 (s).

Synthesis of 11. $FeCl_2(thf)_{1.5}$ (1.15 g, 4.91 mmol) was added in a drybox to a colorless solution of **1** (4.61 g, 5.4 mmol) in THF (300 mL), resulting in a yellow solution, which was reacted for 24 h at room temperature. $CuCl_2(thf)_{0.5}$ (3.6 g, 21.7 mmol) was then added, obtaining a red solution, which was reacted for 24 h. The solvent was removed,

Scheme 2

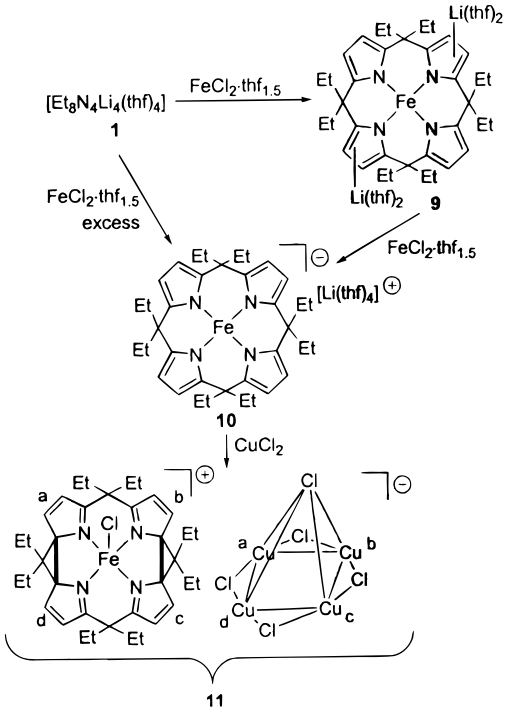

the solid was collected with toluene (250 mL), and the undissolved salts were filtered off. The red solution was concentrated to ∼50 mL and the microcrystalline orange solid filtered and dried (2.7 g, 47%). Anal. Calcd for $C_{36}H_{48}Cl_6Cu_4FeN_4 \cdot (C_7H_8)_{1.5}$, $C_{46.5}H_{60}Cl_6Cu_4FeN_4$: C, 46.61; H, 5.04; N, 4.68. Found: C, 46.18; H, 4.82; N, 4.28. IR (Nujol, ν_{max}/cm^{-1}): 3062 (s), 1536 (m), 1558 (m), 1316 (m), 1059 (m), 1008 (m), 963 (s), 917 (m), 722 (m).

Synthesis of 12. Pyrrole (17.0 g; 250.0 mmol) was added dropwise to a solution of cyclohexanone (24.8 g; 250 mmol) in ethanol (300 mL) cooled to −40 °C and methanesulfonic acid (3 mL), resulting in an amber solution, which was refluxed for 2 h. A white microcrystalline product formed, which was filtered, washed with ethanol, and dried. To remove the excess ethanol, the solid was suspended in Et_2O and stirred overnight, filtered, and dried. Mp > 200 °C. Anal. Calcd for $C_{40}H_{52}N_4$: C, 81.59; H, 8.90; N, 9.51. Found: C, 81.88; H, 8.72; N, 9.41. ^{1}H NMR ($CDCl_3$, 200 MHz, 298 K, ppm): δ 7.08 (bs, 4H, NH); 5.92 (s, 4H, C_4H_2N); 5.90 (s, 4H, C_4H_2N); 1.96−1.89 (m, 16H, C_6H_{10}); 1.54 (m, 24H, C_6H_{10}).

Synthesis of 13. $LiBu^n$ (100 mL, 1.6 M in *n*-hexane, 160 mmol) was added dropwise to a THF (200 mL) suspension of **12** (23.60 g, 40.0 mmol), resulting in a milky suspension, which was refluxed for 2 h, until the release of gas stopped. The solvent was evaporated to dryness at reduced pressure and the white solid collected with *n*-hexane (120 mL), filtered, and dried (30.7 g, 85%). Anal. Calcd for $C_{56}H_{80}Li_4N_4O_4$: C, 74.65; H, 8.95; N, 6.22. Found: C, 74.55; H, 8.35; N, 6.15. ^{1}H NMR (C_6D_6, 200 MHz, 298 K, ppm): δ 6.40 (s, 8H, C_4H_2N);

Scheme 3

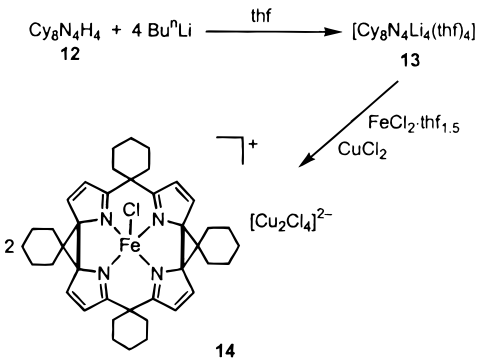

3.27 (m, 16H, THF); 2.71−1.98 (m, 24H, C_6H_{10}); 1.72−1.36 (m, 16H, C_6H_{10}), 1.26 (m, 16H, THF).

Synthesis of 14. $FeCl_2$·$thf_{1.5}$ (1.74 g, 7.4 mmol) was added to a milky suspension of **13** (3.33 g, 3.7 mmol) in THF (250 mL). A red solution was obtained, where a red microcrystalline solid formed rapidly. The mixture was stirred at room temperature for 12 h, then $CuCl_2$·$thf_{0.5}$ (3.25 g, 19.23 mmol) was added, which caused the slow formation of a thin yellow solid. The suspension was reacted for 24 h, then filtered, and the insoluble product was dried (1.5 g, 43%). Crystals suitable for X-ray analysis were grown in CH_3CN. Anal. Calcd for $C_{40}H_{48}Cl_3CuFeN_4$: C, 59.27; H, 5.97; N, 6.91. Found: C, 58.97; H, 6.13; N, 7.02. IR (Nujol, ν_{max}/cm^{-1}): 3080 (s), 1561 (w), 1550 (w), 1528 (w), 1400 (s), 1277 (m) 1211 (w), 1188 (w), 1127 (w), 1061 (m), 1055 (s), 900 (m) 800 (s), 783 (s), 711 (s), 689 (m).

Synthesis of 15, Method A. Degassed Cp_2FeBPh_4 (6.94 g, 13.7 mmol) was added to a solution of **1** (5.85 g, 6.86 mmol) in THF (150 mL) cooled to −40 °C. The solution suddenly turned red, was allowed to reach room temperature, and left to react for 20 h. The solvent was removed at reduced pressure, the solid was collected with benzene (120 mL) and stirred for about 2 h, and then the remaining undissolved solid was filtered off. The solution was concentrated to ∼30 mL, then pentane (∼50 mL) was added, and the solid, which formed, was filtered and dried (2.9 g, 60%). Crystals suitable for X-ray analysis[4] were obtained, recrystallizing the product in THF/heptane. Anal. Calcd for $C_{44}H_{64}Li_2N_4O_2$: C, 76.05; H, 9.28; N, 8.06. Found: C, 75.83; H, 9.03; N, 8.10. ^{1}H NMR (C_6D_6, 200 MHz, 298 K, ppm): δ 6.87 (m, 2H, C_4H_2N); 6.49 (m, 6H, C_4H_2N); 3.25 (m, 8H, THF); 2.53 (m, 4H, CH_2); 2.12 (m, 4H, CH_2); 1.86 (m, 6H, CH_2); 1.61 (m, 2H, CH_2); 1.39 (m, 4H, CH_3); 1.34 (m, 8H, THF); 1.29−0.90 (m, 16H, CH_3); 0.62 (m, 4H, CH_3).

Synthesis of 15, Method B. Complex **1** (0.73 g, 0.86 mmol) was added to a yellow solution of **16** (0.82 g, 0.86 mmol) in THF (70 mL), resulting in a red solution, which was reacted for 12 h. The solvent was removed at reduced pressure, then the residual solid was dissolved in Et_2O (100 mL), and the undissolved salts were filtered off. The solvent was evaporated to dryness and the solid collected with *n*-hexane (80 mL), filtered, and dried (93%). The product was proven by ^{1}H NMR to be **15**.

Synthesis of 16, Method A. Degassed Cp_2FeBPh_4 (5.22 g, 10.32 mmol) was added to a colorless solution of **1** (2.2 g, 2.58 mmol) in THF (120 mL) cooled to −40 °C, resulting in a red solution, which was reacted for 24 h. The solvent was evaporated under reduced pressure, and the impurities were removed by extraction in *n*-hexane. The beige solid was treated with dioxane (200 mL) and stirred for ∼2 h, then some undissolved $LiBPh_4$ was filtered off. The solution was taken to dryness, then the product was collected with *n*-hexane (80 mL), filtered, and dried (1.4 g, 63%). Crystals suitable for X-ray analysis[4] were obtained by recrystallizing the product in THF/hexane. Anal. Calcd for $C_{64}H_{76}BLiN_4O$: C, 82.21; H, 8.19; N, 5.99. Found: C, 82.48; H, 8.17; N, 6.00. ^{1}H NMR ($CDCl_3$, 200 MHz, 298 K, ppm): δ 7.50 (m, 8H, BPh_4); 7.30 (d, J = 4.9 Hz, 4H, C_4H_2N); 7.10 (t, J = 6.8 Hz, 8H, BPh_4); 6.94 (t, J = 6.8 Hz, 4H, BPh_4); 6.55 (d, J = 4.9 Hz, 4H, C_4H_2N); 3.76 (m, 4H, THF); 2.42 (q, J = 7.3 Hz, 4H, CH_2); 2.34 (q, J = 7.3 Hz, 4H, CH_2); 2.15 (q, J = 7.3 Hz, 4H, CH_2); 1.99 (q, J = 7.3 Hz, 4H, CH_2); 1.97 (m, 4H, THF); 1.10 (t, J = 6.8 Hz, 6H, CH_3); 0.93 (t, J = 6.8 Hz, 6H, CH_3); 0.82 (m, 12H, CH_3).

Synthesis of 16, Method B. Degassed Cp_2FeBPh_4 (2.1 g, 4.2 mmol) was added to a red solution of **15** (1.5 g, 2.1 mmol) in THF (100 mL) cooled to −40 °C, resulting in a yellow-red solution, which was reacted for 12 h at room temperature. The solvent was removed at reduced pressure, then the residue solid was suspended in dioxane (100 mL) and stirred for 2 h, and the undissolved $LiBPh_4$ was filtered off. The solvent was evaporated to dryness and the solid collected with *n*-hexane (110 mL), filtered, and dried (1.18 g, 60%). The product was proven by ^{1}H NMR to be **16**.

Synthesis of 17. Degassed Cp_2FeBPh_4 (5.12 g, 10.0 mmol) was added to a yellow solution of **2** (2.14 g, 2.5 mmol) in THF (125 mL) cooled to −40 °C, resulting in a red solution, which was reacted for 24 h at room temperature. The solvent was removed at reduced pressure, and the solid collected with Et_2O (50 mL) and then extracted with fresh Et_2O (120 mL). The mother liquor was concentrated to ∼50 mL and

Scheme 4

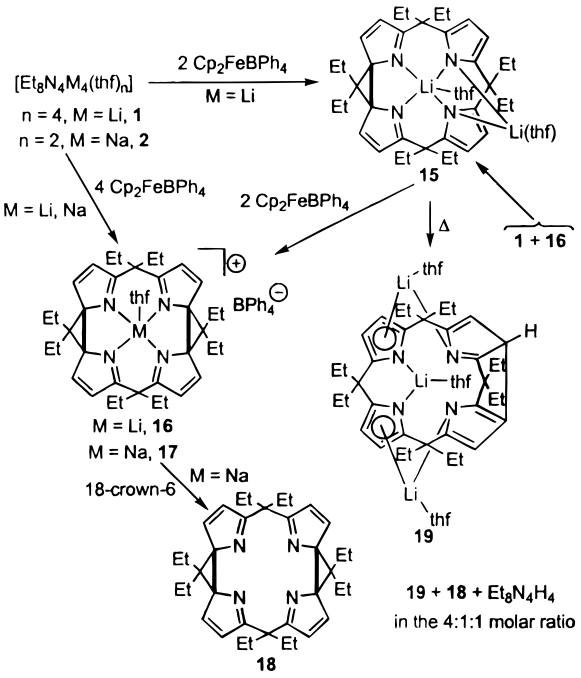

the white solid filtered and dried (2.2 g, 76%). Crystals suitable for X-ray analysis were obtained by slow extraction with Et_2O. Anal. Calcd for $C_{64}H_{76}BN_4NaO$: C, 80.82; H, 8.05; N, 5.89. Found: C, 81.11; H, 8.27; N, 5.78. IR (Nujol, ν_{max}/cm^{-1}): 3055 (s), 1938 (w), 1877 (w), 1816 (w), 1567 (s), 1266 (m), 1137 (m), 1032 (m), 958 (w), 837 (w), 807 (m), 771 (s), 730 (s), 612 (s). ^{1}H NMR (CD_2Cl_2, 200 MHz, 298 K, ppm): δ 7.36 (d, J = 4.9 Hz, 4H, C_4H_2N); 7.33 (m, 8H, BPh_4); 7.02 (t, J = 7.0 Hz, 8H, BPh_4); 6.89 (t, J = 7.0 Hz, 4H, BPh_4); 6.54 (d, J = 4.9 Hz, 4H, C_4H_2N); 3.41 (m, 4H, THF); 2.40 (m, 8H, CH_2); 2.15 (m, 8H, CH_2); 2.01 (m, 4H, THF); 0.96 (m, 12H, CH_3); 0.85 (m, 12H, CH_3).

Synthesis of 18. 18-Crown-6 (0.36 g, 1.35 mmol) was added to an amber suspension of **17** (1.19 g, 1.35 mmol) in benzene (120 mL). The mixture became brighter, while a microcrystalline white solid formed. The mixture was stirred for 12 h, the solid was filtered off, and the solvent was removed at reduced pressure. The residue was collected with *n*-hexane (80 mL), filtered, and dried. Anal. Calcd for $C_{36}H_{48}N_4$: C, 80.55; H, 9.01; N, 10.44. Found: C, 80.65; H, 9.55; N, 10.67. ^{1}H NMR ($CDCl_3$, 200 MHz, 298 K, ppm): δ 7.54 (d, J = 4.9 Hz, 4H, C_4H_2N); 6.77 (d, J = 4.9 Hz, 4H, C_4H_2N); 2.50−2.30 (m, 8H, CH_2); 2.19−1.94 (m, 8H, CH_2); 0.85 (m, 24H, CH_3).

Synthesis of 19, Method A. Degassed Cp_2FeBPh_4 (5.19 g, 10.3 mmol) was added to a colorless solution of **1** (4.38 g, 5.1 mmol) in THF (120 mL) cooled to −40 °C, resulting in a red solution, which was reacted overnight. The solvent was removed at reduced pressure, and the solid was collected with *n*-hexane (80 mL), then extracted with fresh *n*-hexane (120 mL). The mother liquor was concentrated to ∼50 mL, and the red-violet solid was filtered and dried (2.1 g, 59%). Crystals suitable for X-ray analysis were obtained by recrystallizing the product in *n*-hexane. Anal. Calcd for $C_{44}H_{63}Li_3N_4O_2$: C, 75.41; H, 9.06; N, 8.00. Found: C, 75.55; H, 9.11; N, 8.15. ^{1}H NMR (C_6D_6, 200 MHz, 298 K, ppm): δ 6.42 (d, J = 2.4 Hz, 1H, C_4H_2N); 6.34 (m, 2H, C_4H_2N); 6.26 (d, J = 2.4 Hz, 1H, C_4H_2N); 6.19 (d, J = 2.4 Hz, 1H, C_4H_2N); 6.09 (d, J = 2.4 Hz, 1H, C_4H_2N); 4.64 (d, J = 2.4 Hz, 1H, C_4H_2N); 3.44 (m, 8H, THF); 2.49−2.18 (m, 7H, CH_2); 2.01−1.72 (m, 8H, CH_2); 1.52−1.46 (m, 1H, CH_2); 1.26−1.16 (m, 14H, CH_3 + THF); 1.02−0.90 (m, 15H, CH_3); 0.65 (t, J = 7.3 Hz, 3H, CH_3).

Synthesis of 19, Method B. An orange solution of **15** (1.0 g, 1.44 mmol) in benzene (50 mL) was heated at 80 °C. After 3 h, a sample of the bulk of the reaction analyzed via ^{1}H NMR showed the formation of **19**, [$Et_8N_4H_4$], and **18**, with some amount of **15** remaining. After 8 h, **15** disappeared and the three products **19**, **18**, and [$Et_8N_4H_4$] formed in the ratio 4:1:1. Prolonged heating gave rise to the decomposition of

Scheme 5

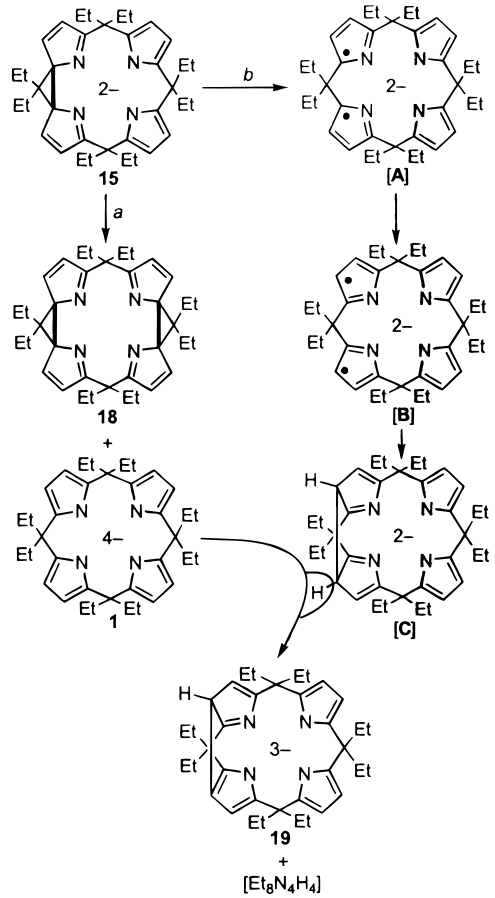

18 and formation of undetectable products, while the thermally stable **19** and $[Et_8N_4H_4]$ were still present.

Synthesis of 21. Degassed Cp_2FeBPh_4 (2.61 g, 5.17 mmol) was added to a yellow solution of **20** (2.32 g, 2.58 mmol) in THF (100 mL) cooled to −40 °C, resulting in a dark red solution, which was stirred for 12 h. The solution was then evaporated to dryness and the product extracted with *n*-pentane (120 mL) to remove insoluble impurities. The residue was dissolved in benzene (80 mL), then dioxane (40 mL) was added to completely precipitate $LiBPh_4$. Salts were filtered off and the red solution evaporated to dryness. The solid was collected with *n*-pentane (80 mL), filtered, and dried (1.00 g; 65%). Anal. Calcd for $C_{36}H_{48}N_4Ni$: C, 72.61; H, 8.12; N, 9.41. Found: C, 72.47; H, 7.85; N, 9.31. IR (Nujol, ν_{max}/cm^{-1}): 3086 (s); 1585 (s); 1300 (s); 1280 (s); 1077 (s); 1022 (s); 807 (s); 735 (s). ^{1}H NMR (C_6D_6, 200 MHz, 298 K, ppm): δ 6.68 (d, J = 4.9 Hz, 2H, C_4H_2N); 6.54 (d, J = 2.9 Hz, 2H, C_4H_2N); 6.33 (d, J = 2.9 Hz, 2H, C_4H_2N); 6.13 (d, J = 4.9 Hz, 2H, C_4H_2N); 3.57 (q, J = 7.3 Hz, 2H, CH_2); 2.85 (q, J = 7.3 Hz, 2H, CH_2); 2.56 (q, J = 7.3 Hz, 2H, CH_2); 2.29 (m, 2H, CH_2); 1.84 (q, J = 7.3 Hz, 4H, CH_2); 1.62 (m, 2H, CH_2); 1.42 (t, J = 6.8 Hz, 6H, CH_3); 1.27 (m, 2H, CH_2); 1.02 (t, J = 7.3 Hz, 6H, CH_3); 0.86 (t, 3H, J = 6.8 Hz, 3H, CH_3); 0.70 (t, J = 7.3 Hz, 6H, CH_3); 0.46 (t, J = 6.8 Hz, 3H, CH_3).

Synthesis of 22, Method A. Degassed Cp_2FeBPh_4 (1.8 g, 3.5 mmol) was added to a THF solution of **20** (3.2 g, 3.5 mmol) cooled to −40 °C, resulting in a dark solution, which was reacted at room temperature for 24 h. The solvent was evaporated, and the yellow solid was treated with benzene (110 mL), stirred for 2 h, and then filtered to remove the undissolved salts. The solvent was evaporated under reduced pressure and the solid collected with *n*-hexane (80 mL), filtered, and dried (1.8 g; 75%). Anal. Calcd for $C_{80}H_{112}Li_2N_8Ni_2O_2$: C, 71.22; H, 8.37; N, 8.31. Found: C, 71.28; H, 8.40; N, 8.56. ^{1}H NMR (C_6D_6, 200 MHz, 298 K, ppm): δ 6.20 (s br, 8H, C_4H_2N); 5.89 (s br, 8H, C_4H_2N); 4.68 (s br, 2H, CH_2); 3.76 (s br, 2H, CH_2); 2.95 (m, 8H, THF); 2.78 (m, 8H, THF); 2.44−1.61 (s br, 20H, CH_2); 1.23 (m, 8H, THF); 1.53−0.85 (s br, 48H, CH_3). The different solvation degrees have been found depending on the drying time in vacuo. The preliminary X-ray analysis showed two THF molecules per lithium, as displayed in Scheme 6, while the microanalysis was carried out on a sample dried for a very long time. The samples used for NMR have different solvation degrees because their preparation was carried out in vacuo. In this specific case, we report the sample with three THF molecules.

Scheme 6

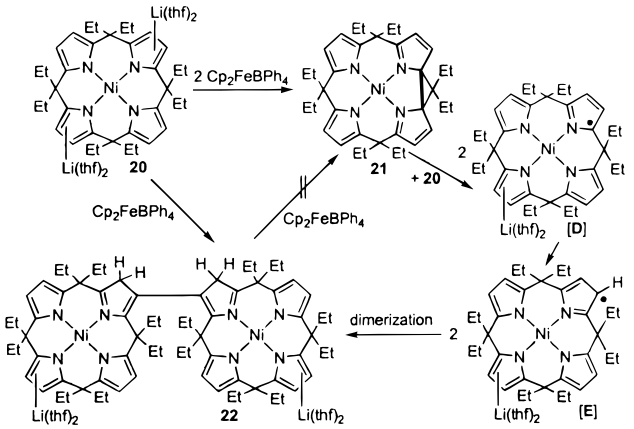

Synthesis of 22 from 20 and 21, Method B. Solid **20** (0.62 g, 1 mmol) and **21** (0.93 g, 1 mmol) were mixed, then THF (70 mL) was added to obtain a red solution, which was reacted for 12 h. The solvent was evaporated and the yellow solid collected with *n*-hexane (50 mL), filtered, and dried. The ^{1}H NMR spectrum showed it to be **22**.

X-ray Crystallography for Complexes 5, 7, 11, 14, and 19. Suitable crystals were mounted in glass capillaries and sealed under nitrogen. The reduced cells were obtained with the use of TRACER.[9] Crystal data and details associated with data collection are given in Tables 1 and S1. Data for **5**, **7**, **11**, and **14** were collected on a single-crystal diffractometer (Siemens AED for **5** and Rigaku AFC6S for **7**, **11**, **14**) at 295 K for **5** and **7** and at 133 K for **11** and **14**. For intensities and background individual reflection profiles were analyzed.[10] The structure amplitudes were obtained after the usual Lorentz and polarization corrections,[11] and the absolute scale was established by the Wilson method.[12] Data for complex **19** were collected at 133 K on a Stoe IPDS area detector. A total of 200 images from $\varphi = 0°$ to $\varphi = 180°$ were recorded, each one exposed for 240.8 s. The diffraction data were indexed and processed using the STOE program package. No absorption correction was deemed necessary.

The crystal quality for all complexes was tested by ω scans showing that crystal absorption effects could not be neglected for **7**, **11**, and **14**. For these complexes data were then corrected for absorption using a semiempirical method.[13] The function minimized during the least−squares refinement was $\sum w(\Delta F^2)^2$. Anomalous scattering corrections were included in all structure factor calculations.[14b] Scattering factors for neutral atoms were taken from ref 14a for nonhydrogen atoms and from ref 15 for H. Structure solutions were based on the observed reflections [$I > 2\sigma(I)$]. The refinements were carried out using the unique total reflections having $I > 0$.

The structures of **5**, **7**, **14**, and **19** were solved by the heavy-atom method starting from a three-dimensional Patterson map. The structure

(9) Lawton, S. L.; Jacobson, R. A. *TRACER (a cell reduction program)*; Ames Laboratory, Iowa State University of Science and Technology: Ames, IA, 1965.

(10) Lehmann, M.S.; Larsen, F. K. *Acta Crystallogr., Sect. A: Cryst. Phys., Diffr., Theor. Gen. Crystallogr.* **1974**, *A30*, 580−584.

(11) Data reduction was carried out on a Quansan personal computer equipped with an INTEL Pentium processor and on an ENCORE 91 computer.

(12) Wilson, A. J. C. *Nature* **1942**, *150*, 151.

(13) North, A. C. T.; Phillips, D. C.; Mathews, F. S. *Acta Crystallogr., Sect. A: Cryst. Phys., Diffr., Theor. Gen. Crystallogr.* **1968**, *A24*, 351.

(14) (a) *International Tables for X-ray Crystallography*; Kynoch Press: Birmingham, England, 1974; Vol. IV, p 99. (b) *Ibid.*, p 149.

(15) Stewart, R. F.; Davidson, E. R.; Simpson, W. T. *J. Chem. Phys.* **1965**, *42*, 3175.

Table 1. Experimental Data for the X-ray Diffraction Studies on Crystalline Complexes **5**, **7**, **11**, **14**, and **19**

	5	**7**	**11**	**14**	**19**
formula	$C_{36}H_{48}MnN_4 \cdot C_{16}H_{32}LiO_4$	$C_{72}H_{96}Cl_{13}Cu_9Mn_2N_8$	$C_{36}H_{48}Cl_6Cu_4FeN_4\ 3C_4H_8O \cdot 0.5C_2H_3N$	$C_{40}H_{48}ClFeN_4 \cdot 0.5Cu_2Cl_4$	$C_{44}H_{63}Li_3N_4O_2$
a, Å	16.181(2)	12.066(1)	14.988(5)	12.571(3)	16.692(3)
b, Å	16.181(2)	15.839(3)	15.614(7)	15.259(5)	12.704(3)
c, Å	39.222(3)	11.248(3)	12.027(4)	10.667(4)	20.709(4)
α, deg	90	97.20(2)	108.44(3)	105.49(2)	90
β, deg	90	92.72(1)	100.32(3)	96.67(2)	111.79(3)
γ, deg	90	87.75(1)	85.78(3)	81.00(2)	90
V, Å^3	10 269(2)	2129.1(7)	2627(2)	1941.6(11)	4048.6(17)
Z	8	1	2	2	4
formula weight	887.1	2216.3	1275.9	831.1	700.8
space group	$I4_1/acd$ (no. 142)	$P\bar{1}$ (no. 2)	$P\bar{1}$ (no. 2)	$P\bar{1}$ (no. 2)	$P2_1/c$ (no. 14)
T, °C	22	22	−140	−140	−140
λ, Å	0.710 69	0.710 69	0.710 69	0.710 69	0.710 69
ρ_{calc}, g cm^{-3}	1.148	1.729	1.613	1.422	1.150
μ, cm^{-1}	2.89	29.38	22.20	11.65	0.64
transmission coeff	0.952−1.000	0.568−1.000	0.874−1.000	0.782−1.000	0.955−1.000
R[a]	0.027	0.062	0.050	0.059	0.055
wR2[b]	0.041	0.188	0.156	0.169	0.139

[a] $R = \sum|\Delta F|/\sum|F_o|$ calculated on the unique observed data [$I > 2\sigma(I)$]. [b] $wR2 = [\sum w|\Delta F^2|^2/\sum w|F_o^2|^2]^{1/2}$ calculated on the unique data having $I > 0$.

of **11** was solved using SHELX-86.[16] Refinements were done by full-matrix least-squares first isotropically, then anisotropically for all the non-H atoms, except for disordered atoms. All hydrogen atoms (except for those associated with the disordered molecules, which were ignored) were located from difference Fourier maps and introduced in the subsequent refinements as fixed atom contributions with isotropic *U*'s fixed at 0.15 for **5**, 0.10 for **7**, 0.08 for **11**, and 0.05 Å^2 for **14** and **19**. In the last stage of refinement the weighting scheme $w = 1/[\sigma^2(F_o^2) + (aP)^2]$ (with $P = (F_o^2 + 2F_c^2)/3$ and $a = 0.0108$, 0.1020, 0.0980, 0.1109, and 0.0696 for **5**, **7**, **11**, **14**, and **19**, respectively) was applied. The final difference maps for **5**, **7**, **11**, and **19** showed no unusual feature, with no significant peak above the general background. In complex **14** the final difference map showed a residual peak of 3.16 e Å^{-3} in the near proximity of Cu(1) along the Cu(1)−Cl(3) bond.

Refinement of complex **7** was carried out straightforwardly. In complex **5** the C(44) carbon atom of the independent THF molecule was found to be statistically distributed over two positions, called A and B, isotropically refined with site occupation factors of 0.65 and 0.35, respectively. In complex **11** the O(3), C(49)−C(52) THF solvent molecule of crystallization was affected by disorder, which was solved by splitting the atoms over two positions, called A and B, isotropically refined with a site occupation factor of 0.7 and 0.3, respectively. During the refinement the C−O and C−C distances of the disordered THF molecule were constrained to be 1.48(1) and 1.54(1) Å, respectively. In complex **14** the acetonitrile solvent molecule of crystallization was found to be disordered over two positions about an inversion center. The N(5), C(41), and C(42) atoms were therefore isotropically refined with site occupation factors of 0.5. In complex **19** the rather high thermal parameters reached by the C(3) and C(7) carbon atoms of adjacent pyrrole indicated the presence of disorder, which was solved by splitting the atoms over two positions, called A and B, isotropically refined with site occupation factors of 0.5.

All calculations were performed using SHELX76[17] for the early stages of solution and SHELXL93[18] for refinements. Final atomic coordinates are listed in Tables S2−S6 for non-H atoms and in Tables S7−S11 for hydrogens. Thermal parameters are given in Tables S12−S16, bond distances and angles in Tables S17−S21.[19]

Table 2. Selected Bond Distances (Å) and Angles (deg) for Complexes **5** and **7**

	5		
Mn(1)−N(1)	1.914(4)		
Mn(1)−N(2)	1.957(3)		
C(1)−C(2)	1.370(6)		
C(6)−C(7)	1.339(5)		
	7		
Mn(1)−Cl(1)	2.321(3)	N(4)−C(16)	1.436(12)
Mn(1)−N(1)	2.214(8)	N(4)−C(19)	1.299(12)
Mn(1)−N(2)	2.239(7)	C(4)−C(5)	1.544(12)
Mn(1)−N(3)	2.214(7)	C(4)−C(6)	1.577(12)
Mn(1)−N(4)	2.222(7)	C(5)−C(6)	1.543(12)
Cu(1)−C(2)	2.116(9)	C(14)−C(15)	1.543(14)
Cu(1)−C(3)	2.120(9)	C(14)−C(16)	1.587(12)
Cu(2)−C(7)	2.158(9)	C(15)−C(16)	1.514(14)
Cu(2)−C(8)	2.119(10)	C(5)−C(4)−C(6)	59.3(6)
Cu(4)−Cu(5)	3.005(2)	C(4)−C(5)−C(6)	61.4(6)
Cu(4)−Cl(4)	2.377(4)	C(4)−C(6)−C(5)	59.3(6)
N(1)−C(1)	1.298(12)	C(15)−C(14)−C(16)	57.8(6)
N(1)−C(4)	1.450(12)	C(14)−C(15)−C(16)	62.5(6)
N(2)−C(6)	1.427(12)	C(14)−C(16)−C(15)	59.6(6)
N(2)−C(9)	1.299(11)		
N(3)−C(11)	1.305(12)		
N(3)−C(14)	1.439(11)		

Results and Discussion

(A) Oxidation Pathway of Manganese−Porphyrinogen. Due to the relevant role of manganese in redox chemistry and its activity in high oxidation states,[20] we examined the synthesis and the oxidation behavior of Mn−porphyrinogen. The synthesis of **3** and **4** (see Scheme 1) has been performed from the corresponding lithium and sodium derivatives, **1**[8,21] and **2**, respectively. The synthesis and characterization of **2** are reported here, while the synthesis and use of **1** are well-defined. The use of **2** displays particular advantages over **1** for the synthesis of transition metal−porphyrinogen complexes, because of the much lower solubility of NaX vs LiX salts in the polar solvents used during the synthesis and for the quite different binding ability of Li^+ vs Na^+ toward the pyrrolyl anions.[4,8,21,22] Therefore, under appropriate conditions we can synthesize either dimetallic [M−Li] or alkali-free transition metal porphyrinogen complexes. Under the experimental conditions used, both **3** and

(16) Sheldrick, G. M. *SHELXL86. Program for the solution of crystal structures*; University of Göttingen, Germany, 1986.

(17) Sheldrick, G. M. *SHELX76. Program for Crystal Structure Determination*; University of Cambridge, Cambridge, England, 1976.

(18) Sheldrick, G. M. *SHELXL93. Program for Crystal Structure Refinement*; University of Göttingen, Göttingen, Germany, 1993.

(19) See paragraph at the end regarding Supporting Information.

(20) (a) *Photosynthesis*; Briggs, W. R., Ed.; ARL: New York, 1989. (b) *The Photosynthetic Reaction Center*, Vol. I and II; Deisenhofer, J., Norris, J. R., Eds.; Academic: New York, 1993. (c) *Manganese Redox Enzymes*; Pecoraro, V. L., Ed.; VCH: New York, 1992. (d) Wieghardt, K. *Angew. Chem., Int. Ed. Engl.* **1989**, *28*, 1153.

(21) De Angelis, S.; Solari, E.; Floriani, C.; Chiesi-Villa, A.; Rizzoli, C. *J. Chem. Soc., Dalton Trans.* **1994**, 2467.

Table 3. Comparison of Relevant Structural Parameters within the Metal-Porphyrinogen Units for Complexes **5**, **7**, **11**, **14**, and **19**

		5	**7**	**11**	**14**	**19**
distance of atoms from the N4 core, Å	N(1)	0.000(−)	0.006(8)	0.001(7)	0.004(3)	-0.005(2)
	N(2)	0.000(−)	−0.004(7)	−0.001(7)	-0.004(3)	0.005(2)
	N(3)		0.006(8)	0.001(7)	0.004(3)	−0.007(2)
	N(4)		−0.004(7)	−0.001(7)	-0.004(3)	0.007(2)
	M[a]	0.000(−)	0.948(2)	0.815(3)	0.869(1)	0.844(4)
distance of M from A,[b] Å		0.000(−)	0.795(2)	0.998(2)	0.994(1)	2.629(5) [2.555(5)][c]
distance of M from B,[b] Å		0.000(−)	0.816(2)	1.036(3)	1.025(1)	2.644(5) [2.703(5)]
distance of M from C,[b] Å			1.016(2)	1.002(3)	0.931(1)	0.465(4)
distance of M from D,[b] Å			1.088(2)	1.052(2)	1.035(1)	0.463(4)
dihedral angles between the N_4 core	(A)	152.6(1)	133.9(3)	130.5(2)	129.4(1)	97.6(1) [101.4(1)]
and the A, B, C, D rings, deg	(B)	151.3(1)	133.7(2)	130.0(2)	128.8(1)	100.7(1) [97.4(1)]
	(C)		127.6(3)	130.1(2)	130.9(1)	123.1(1)
	(D)		125.5(2)	129.2(2)	128.5(1)	124.4(1)
dihedral angle between AB, deg		141.1(1)	119.8(4)	122.3(3)	117.1(2)	92.7(1) [93.2(1)]
dihedral angle between AD, deg		141.1(1)	112.9(4)	107.6(3)	109.6(2)	114.6(1) [116.4(1)]
dihedral angle between BC, deg		141.1(1)	113.7(4)	106.3(3)	110.1(2)	117.3(1) [115.3(1)]
dihedral angle between CD, deg		141.1(1)	111.7(4)	122.2(3)	119.3(2)	170.3(1)

[a] M should be read Mn(1) in **5** and **7**; Fe(1) in **11** and **14**; Li(1) in **19**. [b] A, B, C, and D define the pyrrole rings containing the N(1), N(2), N(3), and N(4) nitrogen atoms, respectively. In **5** N(3) and N(4) should be read N(1)′ and N(2)′, respectively (′ = −0.25+*y*, 0.25+*x*, 0.25−*z*). [c] Values in brackets refer to the A and B pyrrole rings containing C(3)B and C(7)B, respectively.

4 have a dimetallic structure sketched according to the structure reported for other alkali-transition metal complexes, where the alkali cation is η^5-bonded to the peripheral pyrrolyl anions.[6,8,21,22] Both **3** and **4** are very sensitive to air or any other oxidizing agent. The oxidation over a short period of time with molecular oxygen converted **3** to the Mn(III) derivative **5**. Longer exposure to oxygen led to the absorption of up to four moles of O_2 per manganese and did not allow any characterizable compound to be isolated. Unlike in the case of Co−, Ni−, or Cu−porphyrinogen complexes,[2a] oxidation with *p*-benzoquinone did not lead to the expected two-electron-oxidized monocyclopropane derivative. The synthesis of **6** was achieved by the use of 2 equiv of Cp_2FeBPh_4 as the oxidizing agent of **4**. The nature of the oxidizing agent along with that of the alkali cation can have a significant influence on the nature of the oxidized product. The same reaction carried out with the lithium derivative **3** seems to proceed differently, but certainly did not lead to **6**. The reaction of **3** with a controlled amount of $CuCl_2$ led primarily to the Mn(III) derivative, **5**, followed by the oxidation to the biscyclopropane form, **7**. Although an excess of $CuCl_2$ should be used, the formation of **7** from **5** requires formally 3 equiv of oxidizing agent, since the forth one is provided by Mn(III) being reduced to Mn(II). The excess of $CuCl_2$ takes care of the Cl^- not engaged in the reaction, with the formation of counteranions different from $[Cu_9Cl_{11}]^{2-}$. The amount of the latter one forming from "CuCl" determines the maximum yield of **7**. The formation of **7** probably occurs with some amount of other complexes containing the same cation, but different counteranions. The use of an appropriate amount of $CuCl_2$ did not allow us to intercept the intermediate monocyclopropane form **6**, which has been obtained as reported above. On the other hand any attempt to oxidize **6** to **7** using $CuCl_2$ failed. The structure assignment of complexes **3**−**7**, which have the expected analytical, spectroscopic, and magnetic data, has been done according to the analogous Co(II), Ni(II), and Cu(II) derivatives for **3**, **4**, and **6**, while **5** and **7** have been examined with an X-ray analysis.

Selected bond distances and angles for complexes **5** and **7** are presented in Table 2. In Table 3 the most relevant conformational parameters are quoted. The structural parameters concerning the geometry of the atoms related to the formation of cyclopropane are listed in Table 4; the pyrrole rings containing N1, N2, N3, and N4 are labeled A, B, C, and D, respectively.

Table 4. Structural Parameters Related to the Formation of the Cyclopropane Unit in Complexes **7**, **11**, and **14**

	7	**11**	**14**
C(1)···C(19) (Å)	2.453(13)	2.379(12)	2.446(6)
C(4)···C(6) (Å)	1.577(13)	1.621(10)	1.591(6)
C(9)···C(11) (Å)	2.464(13)	2.408(12)	2.442(6)
C(14)···C(16) (Å)	1.588(12)	1.638(10)	1.587(7)
C(4)−C(5)−C(6) (deg)	61.4(6)	63.8(6)	62.7(3)
C(9)−C(10)−C(11) (deg)	108.1(8)	103.7(6)	106.4(3)
C(14)−C(15)−C(16) (deg)	62.5(6)	66.3(5)	62.2(3)
C(1) −C(20)−C(19) (deg)	107.3(8)	101.7(6)	106.5(3)

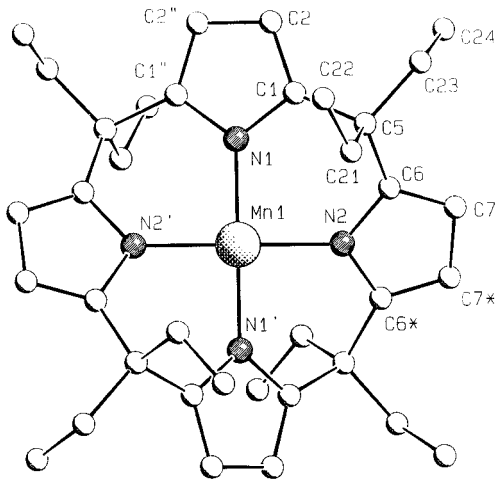

Figure 1. SCHAKAL view of the anion in complex **5**. Prime, double prime, and star denote a transformation of −0.25+*y*, 0.25+*x*, 0.25−*z*; −*x*, 0.5−*y*, *z*; and 0.25−*y*, 0.25−*x*, 0.25−*z*, respectively.

The structure of **5** is shown in Figure 1 and consists of discrete $[Et_8N_4Mn^{III}]^-$ anions and $[Li(thf)_4]^+$ cations. The complex possesses a crystallographically imposed symmetry, manganese lying at the intersection of three 2-fold axes, one of them perpendicular to the N_4 core, and the others running through the Mn−N bonds. The conformation of the complex is close to that observed in $[Et_8N_4Cu^{III}]^-[Li(thf)_4]^{+}$[2a] and in the isostructural

(22) De Angelis, S.; Solari, E.; Floriani, C.; Chiesi-Villa, A.; Rizzoli, C. *Angew. Chem., Int. Ed. Engl.* **1995**, *34*, 1092. Jacoby, D.; Isoz, S.; Floriani, C.; Schenk, K.; Chiesi-Villa, A.; Rizzoli, C. *Organometallics* **1995**, *14*, 4816. Jacoby, D.; Isoz, S.; Floriani, C.; Chiesi-Villa, A.; Rizzoli, C. *J. Am. Chem. Soc.* **1995**, *117*, 2793. Solari, G.; Solari, E.; Floriani, C.; Chiesi-Villa, A.; Rizzoli, C. *Organometallics* **1997**, *16*, 508.

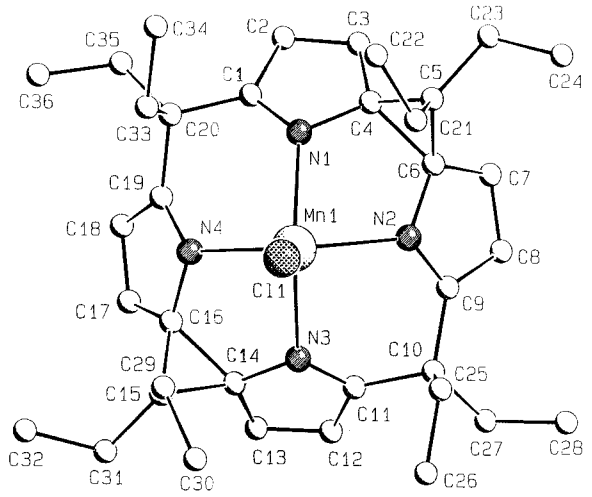

Figure 2. SCHAKAL view of the cation in complex **7**.

$[Et_8N_4Co^{III}]^-[Li(thf)_4]^+$.[23] The N_4 core is planar, with Mn lying in the N_4 plane from symmetry requirements. The manganese atom lies in the plane of the pyrrole rings. The Mn−N bond distances [mean value 1.936(10) Å] are significantly shorter than those quoted in the literature for five- or six-coordinate Mn(III)−porphyrinato species, e.g., 1.998(4)−2.016(4) Å in [Mn(TPP)(CN)],[24] 2.000(4)−2.022(4) Å in [Mn(TPP)(Cl)(Py)],[25] while they are in good agreement with those found in the square planar [Mn(II)(pc)] [1.933(5) Å],[26] where the shortest contact in the axial direction (3.169 Å) involves a nitrogen atom of an adjacent molecule. Bond distances within the pyrrole rings are consistent, with a remarkable double bond localization on C1−C2 [1.370(6) Å] and C6−C7 [1.339(5) Å] (Table 2). The nitrogen atoms do not show any pyramidality. The axial coordination sites around the metal are filled by the *meso*-methylene groups. The two pairs of carbon C21, C21′ and C21″, C21* cap the MnN_4 plane on both sides, their C···C separation being 4.638(13) Å. Four hydrogens, one from each of the aforementioned carbons, provide a flattened tetrahedral cage around the metal (Mn···H61 = 2.80 Å).

The structure of **7** is shown in Figures 2−4 and consists of $[Et_8N_4(\Delta)_2MnCl]^+$ cations, $[Cu_8Cl_9]^-$ anionic aggregates, and $[CuCl_2]^-$ anions in the molar ratio 2:1:1. Figure 2 shows a SCHAKAL top view of the cation. Two centrosymmetric cations are linked in dimers by a $[Cu_8Cl_9]^-$ anion through η^2-interactions involving the Cu1 and Cu2 coppers and the C2−C3 and C7−C8 pyrrole double bonds (Figure 3). The resulting aggregates are held together in infinite chains parallel to the [001] axis by the bridging centrosymmetric $[CuCl_2]^-$ anions. A stereoscopic view of a chain is given in Figure 4. The introduction of cyclopropane units into the porphyrinogen skeleton occurs with the significant structure changes highlighted by a comparison of the structural parameters of **5** and **7** (Table 3). In particular the following has been observed: (i) a remarkable lengthening of the Mn−N bond distances (Table 2); (ii) a strong deviation of the metal from the planar N_4 core (Table 3); (iii) remarkably larger displacements of the metal from the pyrrole rings; (iv) a greater bending of the pyrrole rings around the N_4 core. As can be seen from the data quoted in Table 3, the out-of-plane distance of the metal center from the A and B rings (i.e., those

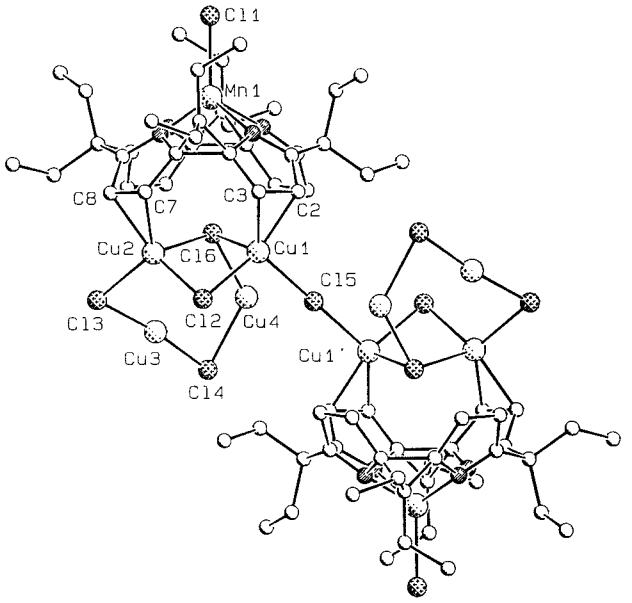

Figure 3. SCHAKAL view of the dimer in complex **7**. A prime denotes a transformation of $-x, -y, -z$.

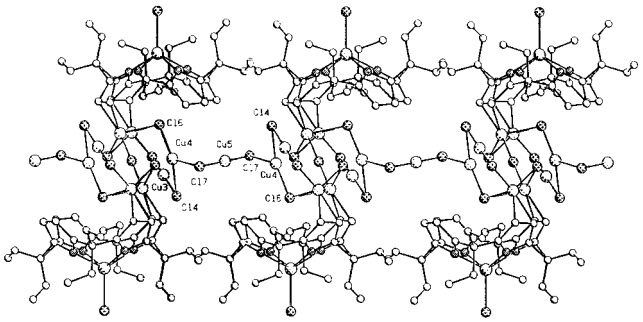

Figure 4. SCHAKAL view of the chain along the [001] axis in complex **7**.

involved in η^2-interaction with the $[Cu_8Cl_9]^-$ anions) is remarkably shorter than for the C and D rings. A small but significant asymmetry is also observed in the bending of pyrrole rings around the N_4 core. Despite these differences, which could be ascribed to the asymmetry of the interactions involving the $Cu_8Cl_9^-$ anion, the complex shows a cone section conformation (like a calix[4]arene) similar to that present in complex **11** and reported for $[Et_8N_4(\Delta_2)FeCl]_2^+[FeCl_4]^{2-}$[2b] and for $[\{Et_8N_4(\Delta_2)CoCl\}\cdots\{Cu_4Cl_5\}]^{2-}$.[2b] This conformation seems to be mainly determined by the presence of the two cyclopropane units. On moving from complex **5** to complex **7**, the N_4 core undergoes a significant deformation from a square of 2.737(4) Å on one edge to a larger rectangle of 2.732(11) × 2.949(11) Å (mean value) in dimension, indicating that the M out-of-plane displacement could not be attributed to a change in size of the N_4 core but mainly to the presence of chlorine in the fifth coordination site. The direction of the Mn−Cl bond is perpendicular to the N4 plane, the dihedral angle it forms with the normal to that plane being 1.9(2)°. The configurations at the asymmetric C4, C6, C14, and C16 carbon atoms are *S*, *R*, *S*, *R*, respectively. Since the space group is centrosymmetric, the enantiomeric diastereoisomer is also present in the structure. The variety of the Cu^I coordination modes should be taken into account to explain the chaining of the molecules. The Cu1 and Cu2 copper atoms show a tetrahedral coordination (wherein the η^2-bonded carbon atoms are considered to occupy one coordination site), while a trigonal coordination is observed for Cu4. The Cu3 and

(23) Floriani, C.; et al. Unpublished results.
(24) Scheidt, W. R.; Lee, Y. J. Luangdibok, W.; Haller, K. J.; Anzai, K.; Hatano, K. *Inorg. Chem.* **1983**, *22*, 1616.
(25) Kirner, J. F.; Scheidt, W. R. *Inorg. Chem.* **1975**, *14*, 2081.
(26) Figgis, B. N.; Mason, R.; Williams, G. A. *Acta Crystallogr.* **1980**, *B36*, 2963.

Cu5 atoms show a diagonal coordination. The four copper atoms in the crystallographically independent $[Cu_4Cl_5]^-$ fragment define an irregular trapezoid whose mean plane (maximum displacement 0.477(2) Å for Cu4) is bent to form a dihedral angle of 38.5(2)° with the N_4 core (Figure 3). As a consequence of the distortion from planarity of the copper atoms (observed in the Fe and Co derivatives), Cl6 is capping only three copper atoms (instead of four) and it is removed from the cavity of the porphyrinogen, the Mn···Cl6 distance being 3.878(4) Å vs 3.154(2) Å in complex **11**, and 3.097(3) Å in [{$Et_8N_4(\Delta)_2Co$}···{Cu_4Cl_5}]. No interaction shorter than 3.48 Å is observed between Cl6 and the carbon atoms. Cl5 lies on a center of symmetry bridging adjacent Cu_4Cl_4 aggregates [Cu1−Cl5 = 2.325(3) Å, Cu1−Cl5−Cu1′, 180°] from symmetry requirements giving rise to the dimer. The Cl2, Cl3, and Cl4 chlorines bridge adjacent Cu atoms of the Cu_4 fragment. The centrosymmetric $CuCl_2^-$ anion (Cu5, Cl7) acts as a bridge between adjacent $Cu_8Cl_9^-$ anions, linking the molecules in chains [Cu5−Cl7, 2.127(4); Cl7−Cu4, 2.331(4) Å].

With the aim to set free the Mn−biscyclopropane form, we tried to remove the Cu(I) cluster from complex **7**. While carbon monoxide and phosphines do not show any reactivity, 2,2′-dipyridyl reacted with it. The reaction led first to the decomplexation of the Cu(I) cluster, followed, however, by the reoxidation of Cu(I) to Cu(II) with concomitant reduction of the cyclopropane units and the formation of the Mn(III)−porphyrinogen **8**. Complex **8** has been characterized by an X-ray analysis, which does not show any real difference with the anion present in complex **5**.[23]

(B) Oxidation Pathway of Iron−Porphyrinogen. The present report gives an exhaustive account of the oxidation of iron, which closely parallels the behavior of Mn and shows significant differences compared with Co, Ni, and Cu. The oxidation pathway of the iron(II)−porphyrinogen complex **9** is shown in Scheme 2. The synthesis of **9** must be carried out with a strictly controlled 1 equiv of [$FeCl_2$·$thf_{1.5}$] since an excess of it leads to the oxidation of **9** to **10**, by a mechanism that is not clear. We suggest, in fact, the unlikely formation of iron(I) reduced species. The synthesis of **10** can be performed reacting **1** with 2 equiv of $FeCl_2$·$thf_{1.5}$ in a single step. The oxidation of **10** with $CuCl_2$ led to the fully oxidized form of porphyrinogen in complex **11**, containing two cyclopropane units within the porphyrinogen skeleton.[23] The explanation of the intriguing stoichiometry is quite similar to that discussed in detail in the case of Mn (see above). The oxidized form of porphyrinogen complexed to the $[Cu_4Cl_5]^-$ cluster is shown in the picture of **11**. When the oxidation by $CuCl_2$ was carried out on **10** prepared in situ, the formation of the copper-free biscyclopropane derivative $[Et_8N_4(\Delta)_2FeCl]^{2+}[FeCl_4]^{2-}$ occurred instead.[2b] The oxidation performed in the presence of the reduced form of $FeCl_2$ has as a major consequence the formation of the copper cluster-free iron−biscyclopropane−porphyrinogen with iron in the oxidation state III rather than II, as it is in complex **11**. In all the oxidations, including those where Cp_2FeBPh_4 was used, we were unable to trap the supposed intermediate monocyclopropane derivative. We should comment that, contrary to what was observed for cobalt, in the case of manganese and iron the monocyclopropane is not necessarily the precursor to the biscyclopropane form. The structure assignment for complex **10** is essentially based on the correct analytical and spectroscopic results and on the close relationship with those of the structurally characterized complexes **5** and [(Et_8N_4Fe){$Li(MeCN)_4$}].[27]

(27) Jacoby, D.; Floriani, C.; Chiesi-Villa, A.; Rizzoli, C. *J. Chem. Soc., Chem. Commun.* **1991**, 220.

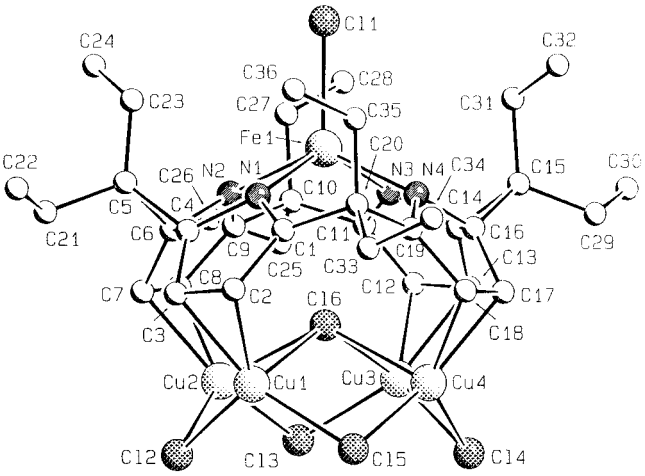

Figure 5. SCHAKAL view of complex **11**.

Table 5. Selected Bond Distances (Å) for Complex **11**

Fe(1)−Cl(1)	2.271(2)	N(2)−C(6)	1.445(10)
Fe(1)−N(1)	2.162(6)	N(2)−C(9)	1.307(8)
Fe(1)−N(2)	2.183(7)	N(3)−C(11)	1.320(8)
Fe(1)−N(3)	2.161(6)	N(3)−C(14)	1.447(12)
Fe(1)−N(4)	2.173(7)	N(4)−C(16)	1.425(10)
Cu(1)−C(2)	2.134(7)	N(4)−C(19)	1.319(9)
Cu(1)−C(3)	2.143(8)	C(4)−C(5)	1.536(14)
Cu(2)−C(7)	2.112(8)	C(4)−C(6)	1.621(10)
Cu(2)−C(8)	2.108(8)	C(5)−C(6)	1.530(12)
Cu(3)−C(12)	2.101(8)	C(6)−C(7)	1.495(10)
Cu(3)−C(13)	2.108(8)	C(13)−C(14)	1.469(10)
Cu(4)−C(17)	2.113(9)	C(14)−C(15)	1.508(11)
Cu(4)−C(18)	2.112(7)	C(14)−C(16)	1.638(10)
N(1)−C(1)	1.292(10)	C(15)−C(16)	1.487(10)
N(1)−C(4)	1.448(11)		

The structure of complex **11** is shown in Figure 5, and selected bond distances and angles are listed in Table 5. It consists of discrete $[Et_8N_4(\Delta)_2FeCl]^+$ cations, $Cu_4Cl_5^-$ anions, and THF molecules as crystallization solvent in the molar ratio of 1:1:3. Each copper(I) is η^2-bonded to the terminal double bonds of the pyrrole rings. The resulting geometry of the molecule shows a cavity having a cone section conformation with two double bonds localized within each pyrrole ring. Complex **11** is isostructural with the corresponding cobalt(III) derivative.[2b] The $Cu_4Cl_5^-$ anion has the framework previously observed with the planar Cu_4 core symmetrically interacting with the four pyrrole rings. The Fe−Cl bond distance (Table 5) is slightly yet significantly longer than that found in $[Et_8N_4(\Delta)_2FeCl]^{2+}[FeCl_4]^{2-}$, while the Fe−N bond distances are in a very good agreement with those found in the same complex. The direction of the Fe−Cl bond is perpendicular to the N_4 plane, the dihedral angle it forms with the normal to that plane being 0.8(2)°.

The most relevant conformational parameters are compared in Table 3 with those of complex **7**, indicating no remarkable differences between them. In these two compounds a strong displacement of the metal atom from the N_4 core is observed along with a strong deformation of the bond angles around the metal, the N−Fe−N angles in the five-membered chelating rings being narrower than those in the six-membered chelation rings. The configurations of the C4, C6, C14, and C16 asymmetric carbon atoms are the same as those observed for complex **7**. The geometry of complex **11** is very similar to that of the $[Et_8N_4(\Delta)_2FeCl]^{2+}$ cation in $[Et_8N_4(\Delta)_2FeCl]^{2+}[FeCl_4]^{2-}$,[2b] which rules out that the cone section conformation of the pyrrole rings could be determined by the copper(I)−η^2-pyrrole interaction.

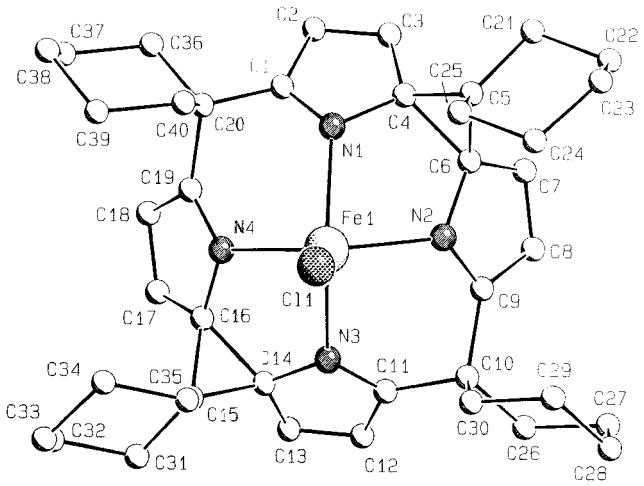

Figure 6. SCHAKAL view of the cation in complex **14**.

Table 6. Selected Bond Distances (Å) for Complex **14**

Fe(1)−Cl(1)	2.249(1)	N(3)−C(14)	1.425(5)
Fe(1)−N(1)	2.171(4)	N(4)−C(16)	1.427(5)
Fe(1)−N(2)	2.183(4)	N(4)−C(19)	1.297(6)
Fe(1)−N(3)	2.154(3)	C(4)−C(5)	1.525(6)
Fe(1)−N(4)	2.187(4)	C(4)−C(6)	1.591(6)
N(1)−C(1)	1.302(6)	C(5)−C(6)	1.531(5)
N(1)−C(4)	1.443(5)	C(14)−C(15)	1.541(5)
N(2)−C(6)	1.422(6)	C(14)−C(16)	1.587(7)
N(2)−C(9)	1.311(5)	C(15)−C(16)	1.532(7)
N(3)−C(11)	1.313(5)		

The only significant difference concerns the Cβ−Cβ distances within the pyrrole rings, averaging 1.377(7) Å in complex **11** and 1.335(10) Å in the $[Et_8N_4(\Delta)_2FeCl]^{2+}$ cation. This small yet significant lengthening could be related to the interactions involving $Cu_4Cl_5^-$, in agreement with the trend of the bond distances observed in complex **7**. The structural features of the $Cu_4Cl_5^-$ anion are very similar to those found in the cobalt derivative.[2b]

The formation of the copper(I) cluster can be avoided, as mentioned earlier, carrying out the oxidation with $CuCl_2$ with the iron(III) porphyrinogen prepared in situ.[2b] This synthetic aspect has been confirmed in the oxidation of the *meso*-octacyclohexylporphyrinogen−iron. The synthetic sequence is shown in Scheme 3. The biscyclopropane form **14** has been isolated free of any copper(I) clusters, while the counteranion is in the present case $[Cu_2Cl_4]^{2-}$ rather than $[FeCl_4]^{2-}$.[2b] The cyclohexyl substituent in the *meso*-carbon does not affect the cyclopropane unit formation.

The structure of **14** is shown in Figure 6. It consists of discrete $[(C_6H_{10})_4N_4(\Delta)_2FeCl]^{2+}$ cations, $[Cu_2Cl_4]^{2-}$ anions, and acetonitrile solvent molecules of crystallization in the molar ratio of 1:0.5:0.5. The $[Cu_2Cl_4]^{2-}$ anion possesses a crystallographically imposed C_i symmetry. The presence of four cyclohexyl groups instead of eight ethyl groups at the *meso*-carbon atoms does not affect the overall geometry of the cation, which as a result is very similar to that observed in complexes **7** and **11** (Table 6). The N_4 core is planar within experimental error, the metal protruding by 0.869(1) Å toward the chlorine atom. The Fe−Cl vector is perpendicular to the N_4 core, the dihedral angle it forms with the normal to the plane being 0.3(1)°. The Fe−Cl(1) bond distance [2.249(1) Å] as well as the Fe−N bond distances [mean value 2.171(8) Å] are in good agreement with those observed in **11**. The bonding sequence shown in Scheme 3 is supported by the structural data (see Table 6). In particular, the Cβ−Cβ average distance [1.337(7) Å] is in agreement with that found in the copper-free cation $[Et_8N_4(\Delta)_2FeCl]^{2+}$. The configurations of the C(4), C(6), C(14), and C(16) asymmetric carbon atoms are *S*, *R*, *S*, *R*, respectively. Since the space group is centrosymmetric, the enantiomeric diastereoisomer is also present in the structure.[28]

(C) Oxidation Pathway of Alkali−Porphyrinogen: The Synthesis of the Metal-Free Biscyclopropane-Porphyrinogens. The results outlined in the previous sections have emphasized the role of transition metal ions in driving the oxidation of the porphyrinogen skeleton to the mono- and biscyclopropane derivatives. The alternative route to use transition metal-free porphyrinogen would perhaps solve the problem of having the biscyclopropane−porphyrinogen available for further complexation with any kind of transition metal. In this perspective, we decided to look to the oxidation of **1** and **2** (see Scheme 4). They undergo a quite clean two-electron oxidation by Cp_2FeBPh_4 to the previously reported monocyclopropane derivative **15**,[2c,4] although the present synthesis is much easier and more convenient. Compound **15** undergoes a further oxidation to **16** by two more equivalents of $[Cp_2FeBPh_4]$. The best synthetic access, however, to the biscyclopropane form is the oxidation of **1** and **2** with 4 equiv of Cp_2FeBPh_4, leading to **16** and **17**, the former one having previously been structurally characterized.[4] The previous synthetic procedure, however, was too complex to become synthetically useful. We should also admit that between the two alkali derivatives, **17** is by far the more accessible by a very simple experimental procedure (see Experimental Section). The sodium cation can be removed from **17** using 18-crown-6, thus obtaining the metal-free biscyclopropane−porphyrinogen, **18**. Although the reaction is feasible, it produces a rather low yield of the desired product. This is mainly due to some instability of the metal-free form of the biscyclopropane−porphyrinogen **18**, although we did not investigate so far its possible rearrangement pathway. It should be emphasized that **15** can be synthesized from equimolar amounts of **1** and **16** (see Experimental Section). This is a quite remarkable reaction, showing how the cyclopropane units can be engaged in intermolecular electron transfers.[2,5] Very likely, this process is assisted by the lithium cation, which can bridge different porphyrinogen units, taking advantage of its coordination mode to the pyrrolyl anion.[5,6,22] Such a redox behavior would be a key point for understanding the thermal rearrangement of **15**. When **15** was heated to 80 °C in *n*-hexane, it rearranges to a mixture of **19**, **18**, and $Et_4N_4H_4$ in a ratio of 4:1:1, as we monitored via NMR spectroscopy. The proposed rearrangement mechanism is depicted in Scheme 5, where the porphyrinogens are drawn as anionic forms rather than associated to lithium cations. Such a rearrangement would follow two pathways, *a* and *b*. The disproportionation of the monocyclopropane form **15** into the biscyclopropane **18** and **1** occurs according to pathway *a*. Complex **19** is derived (pathway *b*) from the conversion of a cyclopropane into a cyclopentane unit across two pyrrolyl anion units. The latter forms from the transposition of a C−C bond between the α-carbon of two adjacent pyrroles into a C−C bond between two β-carbons via the rearrangement of two α-radicals derived from the C−C bond cleavage in the cyclopropane unit (see **A** in Scheme 5), into β-radicals (see **B** in Scheme 5), which then couple leading to **C**. This process is followed by the monodeprotonation of **C** (Scheme 5) by the porphyrinogen tetraanion, **1**, derived from the disproportionation reaction (pathway *a*). Knowledge of the redox and the acid−base chemistry of porphyrinogen will enable one to manage the C−C bond formation. The **15** → **19**

(28) Structural information on the counteranion $[Cu_2Cl_4]^{2-}$ is available as Supporting Information.

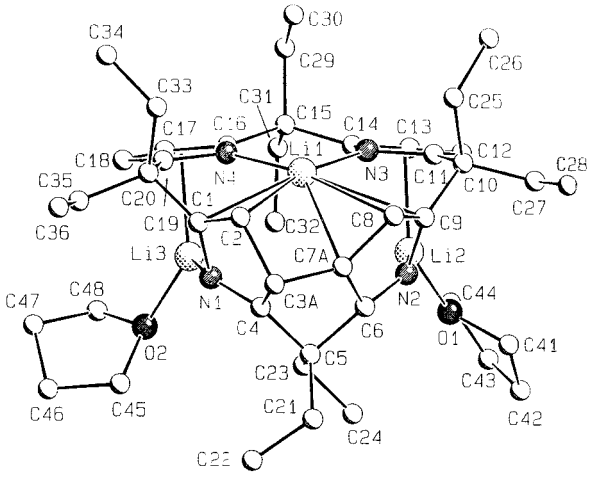

Figure 7. SCHAKAL view of complex **19**. Disorder affecting the C(3) and C(7) carbon atoms has been omitted for clarity.

transformation cannot be reversed upon acidification with PyHCl of **19**. The ^{1}H NMR spectrum of **19** is quite diagnostic of its structure (see Experimental Section) and shows fast proton exchange between the two equivalent β-protons. A crystallographic account of the structure of **19** is reported here.

In the crystal structure both the molecules corresponding to the loss of the hydrogen atom at the C(3) or C(7) carbon atoms are present in the same ratio, resulting in the C(3) and C(7) atoms being distributed over two positions (hereafter referred as *A* and *B*) with site occupation factors of 0.5. The perspective view of complex **19** given in Figure 7 coincides with the C(3) [sp^3] and C(7) [sp^2] atoms occupying their *A* positions. The C−C bond formation between β-carbon atoms gives rise to an unprecedented conformation of the porphyrinogen macrocycle, where the C and D pyrrole rings are nearly parallel [dihedral angle 9.7(1)°] while the A and B rings are strongly tilted upward to be nearly perpendicular [dihedral angle 92.7(1)° and 93.2(1)° for the pyrrole rings containing the C(3) and C(7) carbon atoms in the *A* and *B* positions, respectively]. In comparison with the previous complexes, the conformation of the macrocycle also differs remarkably in the orientation of the A and B pyrrole rings with respect to the N_4 core [dihedral angles $N_4 \wedge$A, 97.6(1)°; $N_4 \wedge$B,100.7(1)°] and in the out-of-plane distance of the central metal cation [Li(1)] from these rings (Table 3). Despite this conformation, the N_4 core maintains its planarity, the Li(1) cation being displaced by 0.844(4) Å (Table 3). The lithium cations exhibit different coordination modes to the trianionic ligand. The Li(1) cation is σ-coordinated to the N(3) and N(4) nitrogen atoms and η-coordinated to the A and B pyrrole rings, the entity of the interaction depending on the presence of the C(3) and C(7) carbon atoms in the *A* or *B* position. When the *A* position is considered, the cation could be described as η^2-coordinated to the A pyrrole ring [Li(1)−C(1), 2.712(5) Å; Li(1)−C(2), 2.771(5) Å; the distances involving the N(1), C(3)A, C(4) atoms are longer than 2.90 Å] and η^3-coordinated to the B pyrrole ring [Li(1)−C(7)A, 2.804(7) Å; Li(1)−C(8), 2.861(6) Å; Li(1)−C(9), 2.786(6) Å; the distances involving the N(2) and C(6) atoms are longer than 2.96 Å]. The opposite situation is observed with the C(3) and C(7) carbons in the *B* position, so a η^3-coordination of Li(1) to the A pyrrole ring [Li(1)−C(1) and Li(1)−C(2) as before; Li(1)−C(3)B, 2.713(6) Å] and a η^2-coordination to the B pyrrole ring [Li(1)−C(8) and Li(1)−C(9) as before] could be proposed. The Li(2) and Li(3) cations achieve a trigonal coordination by σ-bonding one nitrogen atom [N(2) and N(1) for Li(2) and Li(3), respectively] and one oxygen atom from a THF molecule [O(1) and O(2) for Li(2) and Li(3), respectively] and η^5-bonding one pyrrole ring, as indicated by values of the Li−N and Li−C bond distances quoted in Table 7. The trend of bond distances and angles within the C and D pyrrole rings is consistent with a partial double bond localization on the $C_\alpha-C_\beta$ [mean value 1.389(2) Å] bonds and with the single bond character of the $C_\beta-C_\beta$ bonds [mean value 1.415(2) Å]. The configurations of the C(3)A and C(7)B asymmetric carbon atoms are *R* and *S*, respectively. Since the space group is centrosymmetric, the enantiomeric diastereoisomer is also present in the structure.

Table 7. Selected Bond Distances (Å) for Complex **19**[a]

Li(1)−N(3)	1.958(5)	N(1)−C(1)	1.412(2)
Li(1)−N(4)	1.954(5)	N(1)−C(4)	1.329(4)
Li(1)−C(1)	2.712(5)	N(2)−C(6)	1.334(3)
Li(1)−C(2)	2.771(5)	N(2)−C(9)	1.417(3)
Li(1)−C(3)B	2.713(6)	N(3)−C(11)	1.376(3)
Li(1)−C(7)A	2.804(7)	N(3)−C(14)	1.383(3)
Li(1)−C(8)	2.861(6)	N(4)−C(16)	1.376(3)
Li(1)−C(9)	2.786(6)	N(4)−C(19)	1.379(3)
Li(2)−N(2)	2.099(4)	C(3)A−C(7)A	1.531(8)
Li(2)−N(3)	2.332(4)	C(3)B−C(7)B	1.534(8)
Li(2)−Cp(C)	2.077(4)	C(4)−C(5)	1.521(3)
Li(3)−O(2)	1.946(5)	C(5)−C(6)	1.533(4)
Li(3)−N(1)	2.079(4)	C(6)−C(7)A	1.442(5)
Li(3)−N(4)	2.296(5)	C(6)−C(7)B	1.521(6)
Li(3)−Cp(D)	2.092(4)		

[a] Cp(C) and Cp(D) refer to the centroids of the C and D pyrrole rings, respectively.

(D) One- vs Two-Electron Oxidation Pathway: Intra- and Intermolecular C−C Bond Formation. The results so far reported, related to the oxidation of metal−*meso*-octaalkylporphyrinogen complexes, showed that the formation of mono- and biscyclopropane derivatives are overall two- and four-electron oxidation processes.[2−4] When the appropriate transition metal ions are used, namely, Cu and Co, it is possible to single out the two monoelectronic steps leading to the formation of a cyclopropane moiety.[2a] The first one occurs with the oxidation of the metal(II) to metal(III), while in the second step the formation of the cyclopropane reduces the metal back to metal(II).[2a] Our concern was the one-electron oxidation of a porphyrinogen complex containing a metal such as Ni(II), which does not usually undergo a change of oxidation state. This was attempted in the past using *p*-benzoquinone, $CuCl_2$, or other oxidants but did not lead to successful results. The use of Cp_2FeBPh_4, however, enabled us to identify the monoelectronic oxidation of Ni(II)−*meso*-octaethylporphyrinogen, **20** (see Scheme 6). The overall reaction is an oxidative dimerization of **20** occurring via the C−C bond formation between the pyrrole β-carbons of two different units, thus ending up with **22**. The proposed structure of **22** is supported by analytical and spectroscopic data, including an X-ray analysis, which is not reported due to the rather low quality, but which undoubtedly shows the proposed atom connectivity. When the oxidation of **20** was carried out with 2 equiv of Cp_2FeBPh_4, the expected monocyclopropane derivative **21**[2a] formed in a good yield. Complex **22** should not be considered, however, an intermediate to **21**, which does not form from **22**, reacted with two more equivalents of Cp_2FeBPh_4. The results mentioned here and in the previous section suggest a plausible mechanism leading either to the intramolecular or intermolecular C−C bond formation. We should admit that the primary monoelectronic oxidation product should be the α-radical, as expected from the reactivity of the pyrrole,[29] followed by a rather fast oxidation

(29) Gilchrist, T. L. *Heterocyclic Chemistry*, 2nd ed.; Longman: Essex, U.K., 1992. Eicher, T.; Hauptmann, S. *The Chemistry of Heterocycles*; Thieme: Stuttgart, Germany, 1995.

to the monocyclopropane derivative **21**. Therefore, the formation of **22** would not occur via the rearrangement of the α- to the β-radical at the pyrrole ring. The former one would be intercepted by the oxidant before rearranging to the β, which would couple to **22**. In addition, the high yield of **21** from the oxidation of **20** with 2 equiv of Cp_2FeBPh_4 rules out two, intra- and intermolecular, parallel pathways. The answer to the question how complex **22** originates comes from its formation from a reaction carried out mixing an equimolar amount of **20** and **21** in THF at room temperature. This reaction is particularly relevant for a number of reasons. First, it shows the ease of intermolecular electron transfer processes that we believe to be assisted by alkali cations, mainly lithium ions, which are able to bridge porphyrinogens in a different oxidation state, via rather strong ion−pyrrole interactions.[5,8,21,22] Therefore, the formation of the two-electron-oxidized form of the porphyrinogen containing a cyclopropane seems to precede any other oxidized forms. The reaction between **20** and **21** should produce the α-radicals [**D**] (see Scheme 6), which rearrange to the β-radicals [**E**], which ends coupling to form **22**. The coupling reaction followed by the hydrogen shift to the C−C adjacent positions is quite general in the acid−base chemistry of porphyrinogen. In the preceding section we found that the thermally induced rearrangement of **15** to **19** requires the C−C bond cleavage of the cyclopropane in **15**, rearrangement of α- to β-radicals (see Scheme 5), which couple intramolecularly producing **19**. The reactions in Scheme 6 show an important synthetic consequence of the one-electron oxidation of the porphyrinogen tetraanion, namely, the oxidative coupling leading to C−C bond linked dimers. The results reported in this section and in the preceding one serve to clarify the role of the transition metal and the oxidizing agent in driving the oxidation of the porphyrinogen tetraanion. The choice of the metal-oxidizing agent couple is particularly crucial. *p*-Benzoquinone and $CuCl_2$ cannot be employed in the case of the lithium derivative. Under the conditions of using the same innocent oxidant, i.e. Cp_2FeBPh_4, mono- and biscyclopropane form regardless of the presence of a transition metal or an alkali cation. In the latter case, we were, however, unable to detect compounds derived from an overall one-electron oxidation process. In the case of transition metals we have to distinguish between metals that usually do not change oxidation state in the coordination environment determined by the porphyrinogen skeleton, i.e., Ni(II), and those that have different easily accessible oxidation states. In the latter case, the stepwise formation of cyclopropane is assisted by the one-electron redox chemistry at the metal, and we do not really achieve nor see the overall one-electron oxidation of the porphyrinogen ligand. In the case of nickel, the overall one-electron oxidation, through the mechanism outlined above, leads to the oxidative C−C coupling between two metallaporphyrinogen moieties. This is a quite important pathway, which, coupled with the deprotonation reaction,[30] will allow the formation of dimeric, oligomeric, and polymeric metallaporphyrinogen complexes.

(30) Bonomo, L.; Solari, E.; Floriani, C.; Chiesi-Villa, A.; Rizzoli, C. *J. Am. Chem. Soc.* **1998**, *120*, 12972.

Precedents in intermolecular oxidative coupling between two macrocycles such as tmtaa [tmtaa = dibenzotetramethyltetraaza-[14]annulene] are known, although the dimerization always occurs via the *meso*-carbons.[31] Analogous coupling through *meso*-carbons was proposed earlier for the dimerization of metallaporphyrin π-cation radicals.[32] The dimerization via a direct link between pyrrole is characteristic of fully *meso*-alkylated forms, as in the case of *meso*-octaalkylporphyrinogens.

Conclusions

The oxidations carried out on metalla-*meso*-octaalkylporphyrinogens follow different pathways as a function of the metal and the metal−oxidant couples. The use of Cp_2FeBPh_4 allowed the oxidation to be carried out on both transition metal and alkali-metal derivatives and to distinguish between one- and two-electron processes. Regardless of the metal and the porphyrinogen/oxidant ratio, all of the reactions ended in intra- or intermolecular C−C bond formation. The precursor for the different pathways is the cyclopropane functionality, which can, eventually, rearrange. Such rearrangements require intermolecular electron transfers between metallaporphyrinogen units which are assisted by alkali cations. The consequence of such rearrangements are (i) intramolecular C−C bonds different from cyclopropane and (ii) the formation of C−C-bonded metallaporphyrinogen dimers. The latter result opens the methodology for the synthesis of dimeric, oligomeric, and, maybe, polymeric forms of porphyrinogen. Studying the oxidation of Mn(II)−Fe(II)−porphyrinogen, we succeeded in isolating Fe(II)−, Fe(III)−, and Mn(II)−biscyclopropane−porphyrinogen complexes. The oxidation of alkali cation porphyrinogen complexes was found to be the best synthetic access to biscyclopropane−porphyrinogens available for the complexation of any metal and, for the first time, to the metal-free biscyclopropane−porphyrinogens. We should emphasize the potential of the reversible bond formation and cleavage within the porphyrinogen skeleton, which functions as a sort of molecular battery for storing and releasing electrons.

Acknowledgment. We thank the "Fonds National Suisse de la Recherche Scientifique" (Bern, Switzerland, Grant No. 20-53336.98) and Ciba Specialty Chemicals (Basel, Switzerland) for financial support.

Supporting Information Available: ORTEP drawings, tables giving crystal data and details of the structure determination, bond lengths, bond angles, anisotropic thermal parameters, and hydrogen atom locations for **5**, **7**, **11**, **14**, and **19**. This material is available free of charge via the Internet at http://pubs.acs.org.

JA982178F

(31) (a) Mountford, P. *Chem. Soc. Rev.* **1998**, *27*, 105. (b) Dabrowiak, J. C.; Fisher, D. P.; McElroy, F. C.; Macero, D. J. *Inorg. Chem.* **1979**, *18*, 2304, and references therein. (c) Bailey, C. L.; Bereman, R. D.; Rillema, D. P. *Inorg. Chem.* **1986**, *25*, 3149, and references therein.

(32) Balch, A. L.; Noll, B. C.; Reid, S. M.; Zovinka, E. P. *J. Am. Chem. Soc.* **1993**, *115*, 2531.